

Article

Infrared Thermography to Evaluate Thermal Comfort under Controlled Ambient Conditions

Ricardo M. S. F. Almeida ^{1,2,*} , Eva Barreira ² , Maria Lurdes Simões ²  and Tiago S. F. Sousa ²

¹ Department of Civil Engineering, School of Technology and Management of the Polytechnic Institute of Viseu, 3504-510 Viseu, Portugal

² CONSTRUCT-LFC, Department of Civil Engineering, Faculty of Engineering, University of Porto, 4200-465 Porto, Portugal

* Correspondence: ralmeida@estgv.ipv.pt

Abstract: Infrared thermography (IRT) is often used to assess body temperature and can be useful as a diagnostic tool to detect human diseases. Despite this clear application in medicine, some studies can be found in the literature pointing to the use of IRT to measure body temperature as a parameter to evaluate thermal comfort inside buildings. However, there are still some issues that are understudied that this paper tried to address. For this purpose, an intensive experimental campaign was carried out, in which different combinations of temperature and relative humidity were implemented. Thermal images were taken of the face of a young adult, while the air temperature and relative humidity were assessed, as well as the body temperature, using traditional means. The results confirmed that different IR cameras and different ambient conditions (air temperature) impact the image resolution and definition. A linear correlation between the IRT results and the PMV was found for six subregions of the face. This correlation was higher in the forehead, cheekbones, and chin, and less interesting when measuring the temperature of the nose. However, if the overall temperature of the face is assessed, a good agreement between the PMV and the IRT results can still be found, indicating that the average facial temperature can be used as an indicator for the determination of thermal comfort. A prediction model for PMV based on IRT was proposed, with a root mean square error close to 0.70, when applied in a face temperature range between 28.9 °C and 34.4 °C.

Keywords: infrared thermography; thermal comfort; comparison of infrared cameras; face temperature; PMV



Citation: Almeida, R.M.S.F.; Barreira, E.; Simões, M.L.; Sousa, T.S.F.

Infrared Thermography to Evaluate Thermal Comfort under Controlled Ambient Conditions. *Appl. Sci.* **2022**, *12*, 12105. <https://doi.org/10.3390/app122312105>

Academic Editor: Jing Zhao

Received: 7 November 2022

Accepted: 23 November 2022

Published: 26 November 2022

Publisher's Note: MDPI stays neutral with regard to jurisdictional claims in published maps and institutional affiliations.



Copyright: © 2022 by the authors. Licensee MDPI, Basel, Switzerland. This article is an open access article distributed under the terms and conditions of the Creative Commons Attribution (CC BY) license (<https://creativecommons.org/licenses/by/4.0/>).

1. Introduction

Infrared thermography (IRT) is a non-intrusive method for measuring the surface temperature of an object. The non-destructive nature of IRT widens its range of applications, such as in medicine, building diagnostics, electric inspections, or mechanical inspections [1].

The measurement of skin temperature using IRT is a viable and promising method that can be useful for the detection of fever and can potentially contribute to early diagnoses during pandemic crises, such as for SARS-CoV-2 [2,3]. Other medical purposes using IRT are feasible, such as in thermoregulation studies, breast cancer detection, the diagnosis of diabetic neuropathy and vascular disorders, dental diagnostics, blood pressure monitoring, the diagnosis of rheumatic diseases, the diagnosis of dry eye syndrome and ocular diseases, the diagnosis of liver diseases, treatments of the kidneys, heart operations, gynecology, personality testing, and brain imaging [3]. This technique has also been used to determine skin temperature variations while running [4].

1.1. Skin Temperature

Skin temperature is a key parameter for thermal comfort evaluations. Nevertheless, measuring skin temperature can be a complicated task, and several authors have carried out research to assess and propose methods for accurate assessments. Takada et al. [5] used

the skin temperatures measured with thermocouples located in different positions on the body and the time differential as the base of a new model for the prediction of transient thermal sensations during sedentary and walking conditions. The results indicated a good correlation between the predicted thermal sensations and the experimental results, validating the proposed model. Liu et al. [6] also used thermocouples bonded to the body in several locations to find the most suitable ones to assess human thermal comfort. In this study, the reliability, sensitivity, and number of measurement locations were used to interpretate the results. The authors concluded that the calculation of the mean skin temperature using 10 locations was the most appropriate approach. Years later, Liu et al. [7] conducted a similar study to investigate whether the mean skin temperature could also be used to assess individual thermal sensations at high environmental temperatures. The results proved it possible to use it beyond the range of current air temperatures.

Instead of thermocouples, Choi and Loftness [8] assessed body temperatures using a sensor device that consisted of an exposed thermistor with rapid response rates, which measured the skin temperatures in contact with the skin surface by absorbing heat through conduction. As in other studies, the main purpose of this study was investigating the possibility of using body skin temperatures measured in multiple locations to assess thermal sensations.

Chaudhuri et al. [9,10] assessed the possibility of using only a single body location to evaluate the overall thermal state and predict the thermal comfort of the occupants. The selected location was the area between the wrist and the fingers on the dorsal side of the hand, because in this zone the arteries that channel heat loss from the body's core to the periphery meet. The skin temperatures were recorded using a contact sensor device connected to a microcontroller board, which converted the captured signals to skin temperature levels.

In the experimental campaign carried out by Sakoi et al. [11], the skin temperatures in several locations were measured to investigate both the overall thermal comfort and the local discomfort under various asymmetric radiance conditions. In addition to the skin temperature in 25 points of the body, the tympanic temperature, measured with radiative thermometer, and oral temperature, using a disposable thermometer, were also considered in this study. The authors concluded that the local skin temperatures changed depending on the environmental and thermal conditions, even if the mean skin temperature remained almost the same, highlighting the importance of also using the skin temperature distribution to express thermal comfort in heterogeneous environments.

From the studies previously discussed, it is possible to point out that the most used methods for the determination of skin temperature required contact (e.g., thermocouples and temperature sensors bonded to the skin, digital thermometers that take temperature readings in the mouth, tympanic thermometers measuring the temperature inside the ear canal through infrared ray technology, and wristband sensors that assess the temperature of the body by contact with the wrist), being mostly intrusive procedures. Therefore, the use of IRT as a non-intrusive method of thermal comfort assessment is an interesting possibility that is now starting to be studied by the scientific community.

1.2. Assessing Thermal Comfort via IRT

The impact of skin temperature on the thermal sensation has been studied by several authors, and some also proposed methodologies to correlate the two. Aryal et al. [12] explored the suitability of using ambient air sensors, wrist skin temperature using wearable sensors, and IRT to measure different regions of the face (i.e., forehead, nose, left and right cheekbones) to predict individual thermal sensations. The experiment was conducted in a controlled and uniform environment with changes in air temperature from 19 °C to 29 °C. During the measurements, the feedback of the participants regarding the thermal sensations was collected. The results indicated that the models using ambient temperature data presented higher accuracy (about 81%) in predicting thermal comfort when compared to using the measurements from the wrist sensor (about 76%) or the temperatures of the

face quantified via IRT (about 75%). However, when combining the ambient temperature data with the data obtained with the sensor or with IRT, the prediction accuracy increased to about 83%, and when all data were combined the accuracy increased to about 85%. According to Metzmacher et al. [13], the skin temperatures are similar when measured through a PT100 platinum resistance thermometer and an infrared camera. In order to compare the accuracy of both methods, a single tracking point was selected (the center of the forehead). Furthermore, the disadvantages of the contact measurements were detected, such as the effects of physical pressure, the insulation effect due to the fitting material, and the thermal inertia of the sensor.

The body region used to assess the skin temperature is also an open issue. This aspect includes the necessary compatibility between the feasibility of the measurement and its accuracy. The face temperature has been selected by most of the researchers for studies using IRT in the assessment of thermal comfort. According to Ghahramani et al. [14], this region is of interest because there is a high density of blood vessels on the areas around the face, and additionally this body area is not usually covered by clothing when inside buildings. According to the literature review, the evaluations of facial temperatures using IRT are usually focused on specific regions, such as the nose, the cheekbones, and the forehead [12,15]. Other regions of interest were considered by Ghahramani et al. [14,16], who assessed the temperatures of the ears. Metzmacher et al. and Tejedor et al. [13,17] measured the temperature of the chin. Metzmacher et al. [13] evaluated the temperatures of the mouth, the eye, and the inner eye corner, and Cosma et al. [18] studied the face as a whole. These works have shown that different areas of the face behave differently during the heating phase, the cooling phase, and in steady-state conditions. Metzmacher et al. [13] detected the highest temperature in the inner eye corner, followed by the center of the forehead, which presented a more homogeneous temperature distribution. The authors also found more variability in the cheekbones.

Another application of IRT in the study of thermal comfort is the measurement of clothing temperatures. Metzmacher et al. [13] explored the influence of clothing layers using the chest region for the measurements. Four different combinations were assessed: (i) no clothes; (ii) shirt; (iii) sweater; (iv) winter jacket. The skin temperature (no clothes) corresponded to the highest value of the four combinations, with the temperature decreasing from (i) to (iv), i.e., higher insulation resulted in lower measured layering temperatures. Tejedor et al. [17] studied the thermal neutrality of the clothing temperature as well as the skin temperature (resulting from the average of four facial points, i.e., the nose, cheekbones, forehead, and chin), reaching values of 31 °C and 35 °C, respectively. Cosma et al. [18] examined skin and clothing temperatures from different locations that are normally visible in an office context (e.g., the arms, face, and chest), reaching the conclusion that those measurements are correlated with thermal comfort.

The possibility of evaluating thermal comfort through IRT opens space for several innovative applications. Loredan et al. [19] evaluated the thermal properties of ten tabletop materials as well as user perceptions of those materials after use. Li et al. [20] carried out a study to improve the thermal comfort of building occupants by dynamically determining the optimum room conditioning mode and HVAC settings. More recently, Li and Chen [21] developed a new control strategy for HVAC systems that adjusts the thermostat setpoint according to the clothing level and mean facial skin temperature using an image classification model. IRT images were used by Li et al. [22] to recognize age and gender, and the data were applied as inputs in a new non-intrusive method of predicting personal thermal comfort. Yi et al. [23] compared three approaches to thermal comfort modelling for older care home residents: PMV, adaptive comfort, and long wave IRT.

One must stress that the use of IRT in humans requires the standardization of the protocols and a subsequent data analysis. Fernandez-Cuevas et al. [24] divided the influential factors of IRT in humans into three main categories: (i) environmental, i.e., those associated with the location where the study is performed (room size, ambient temperature, relative humidity, atmospheric pressure, source radiation); (ii) individual, i.e., those associated with

the personal characteristics of the person being targeted (intrinsic factors, extrinsic factors); (iii) technical, i.e., those associated with the equipment used (validity, reliability, protocol, camera features, ROI selection, software, statistical analysis). Regarding the environmental factors, most of the studies were carried out in small rooms, under uniform and controlled conditions. In the studies with a focus on IRT of the face, the air temperatures varied from 18 °C to 29 °C [12,14–16,18]. Additionally, the relative humidity rates also showed narrow intervals, varying from 33% to 55% [16,18].

1.3. Gap and Objective

Although previous studies have indicated that IRT can be used to measure body temperature as a parameter to evaluate thermal comfort, some issues remain unclear. A step forward is attempted with this work, which innovates both in the methodological setup and in the data analysis. Concerning the setup, the effects of ambient conditions and the impacts of different characteristics of the IR cameras are discussed. To this end, broader temperature and relative humidity intervals are tested and the results of two distinct IRT devices are compared. Furthermore, in the data analysis, the importance of the area considered for the measurements is analyzed and a correlation between the PMV model and the results of the IRT is tested as a first step for the definition of a model that allows estimations of thermal comfort solely based on IRT measurements.

2. Framework

2.1. Methodology

The methodology was outlined to fulfil the proposed objectives and consisted of carried out a preliminary step to evaluate the applicability of IRT to assess thermal comfort by defining the test protocol and the impacts of the ambient conditions and characteristics of the IR cameras on the results. Only if this first step is accomplished with success can new procedures be defined to achieve generalization. This first stage was based on a large-scale experimental campaign, in which the temperatures of the face were assessed, considering 99 different combinations of ambient conditions (air temperature and relative humidity) and using 2 IR cameras. Only one young adult participated in this study for the sake of clarity and for the ease of implementation. The results obtained were afterwards analyzed in two phases: in phase I, qualitative and quantitative approaches were implemented to compare the results of the two IR cameras; in phase II, we discussed the applicability of the IR images for assessing thermal comfort and tested a possible correlation with the PMV model.

2.2. Equipment

The experimental campaign took place inside a walk-in climatic chamber with dimensions of 2.00 m × 2.00 m × 1.20 m. The temperatures ranged from 50 °C to 180 °C with an accuracy rate of ±0.5 °C and the relative humidity rates ranged from 10% to 98% with an accuracy rate of ±2%. Two IR cameras were used during the procedures, with distinct characteristics, as detailed in Table 1. To confirm the interior ambient conditions, the air temperature and relative humidity inside the climatic chamber were measured using a portable sensor with an accuracy rate of 0.024 °C and resolution rate of ±0.21 °C for the temperature and an accuracy rate of ±2.5% and resolution rate of 0.01% for the relative humidity. Additionally, to evaluate the body temperatures, two commercial thermometers were used—one that requires contact, with a temperature range of 32 °C to 42.9 °C and an accuracy range of ±0.1 °C to 0.2 °C, and another that does not require contact, with a temperature range of 35 °C to 42 °C and an accuracy rate of ±0.2 °C.

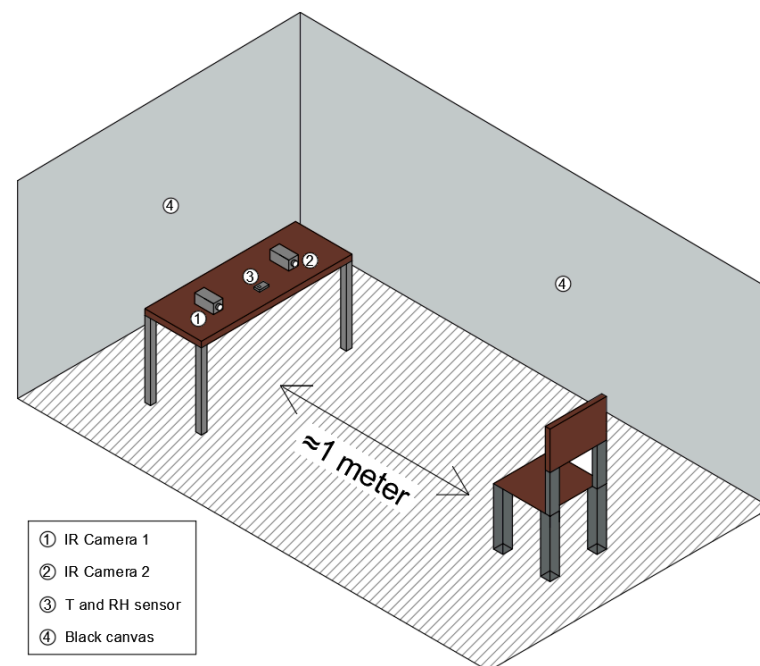
Table 1. IR camera characteristics.

	IR Camera 1	IR Camera 2
Temperature range	−20 °C to 100 °C	−20 °C to 400 °C
Accuracy	±2 °C or 2%	±2 °C or 2%
Thermal sensitivity	0.06 °C at 30 °C	≤0.045 °C at 30 °C
IFOV	1.2 mrad	1.86 mrad
Infrared resolution	320 × 240 pixels	320 × 240 pixels
Field of view	20.1° × 22.7°	34.1°H × 25.6°H
Minimum focus distance	30 cm	<46 cm
Infrared spectral range	8 to 14 μm	7.5 to 14 μm

2.3. Experimental Campaign

In the experimental campaign, the face temperature of a 24-year-old male was assessed using IRT and the emissivity of the skin was 0.98 [17]. To evaluate the influence of the ambient conditions, several scenarios were created. To this end, the air temperatures varied between 10 °C and 30 °C, with increments of 2 °C, while the relative humidity values varied between 40% and 80%, with increments of 5%, leading to a total of 99 different combinations of ambient conditions. The inputs in the climatic chamber were designated as the T_{SP} (temperature setpoint) and RH_{SP} (relative humidity setpoint).

Figure 1 shows a schematic representation of the setup inside the climatic chamber, showing the position of the equipment and the location of the individual. The inner metallic surfaces of the climatic chamber were covered with black canvas to prevent reflection problems. The limitations of the space inside the climatic chamber resulted in a different framing of the head of the individual in the images taken by each IR camera.

**Figure 1.** Schematic representation of the setup inside the climatic chamber.

The experimental procedure implemented for each scenario is schematically represented in Figure 2. The full duration of each test was approximately 50 min. The procedure started with the programming of the climatic chamber with the setpoint conditions (T_{SP} and RH_{SP}), followed by the stabilization of the indoor environment for approximately 30 min. After that period, the individual under study entered the climatic chamber, initiating the acclimatization process, which took about 10 min. During that period, the necessary calibrations of the IR cameras and the assessment of the reflected temperature,

through the procedure described in the standard ASTM: E 1862-97 [25], were conducted. The reflected temperature is the temperature of the energy incident upon and reflected from the surface under study, which can cause measurement errors if not considered and compensated for during data treatment [26]. Finally, the thermal image was captured through an automatic procedure.

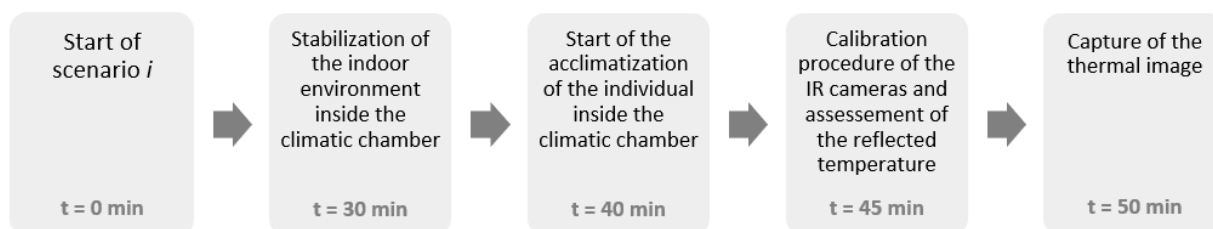


Figure 2. Set of procedures in each tested scenario.

Since the range of the temperature setpoints was substantial [$10\text{ °C} \leq T_{SP} \leq 30\text{ °C}$], the individual's clothing was adapted to the T_{SP} . This adaptation process targeted the chest area as follows: (i) T_{SP} : 10 °C to 14 °C , t-shirt + sweater + coat; (ii) T_{SP} : 16 °C to 24 °C , t-shirt + sweater; (iii) T_{SP} : 26 °C to 30 °C , t-shirt.

Additionally, the measurements of the core temperature using the thermometers were carried out for the RH_{SP} 40%, 60%, and 80% conditions. The measurements occurred after the acclimatization period of 10 min, immediately before capturing the thermal images. The contact thermometer measured the temperature inside the mouth and the non-contact thermometer measured the temperature in the center of the forehead.

2.4. Data Analysis

2.4.1. Phase I: IR Camera Comparison

The comparison of the IR cameras included qualitative and quantitative approaches. Initially, a qualitative analysis of the images was performed, with the focus being the detection of variations in facial temperature in different ambient conditions. To achieve this, the thermal images captured with the two IR cameras for the same T_{SP} and RH_{SP} were compared.

Afterwards, the quantitative analysis included (i) the impact of the ambient conditions on the superficial temperature, (ii) the detection of the location of the hottest point, and (iii) a statistical analysis. For each thermal image, the value and location of the hottest temperature measured on the face were selected for the subsequent data analysis (i.e., $T_{max\ 1}$ —temperature of the hottest point measured by IR camera 1; $T_{max\ 2}$ —temperature of the hottest point measured by IR camera 2). The ambient conditions used in the quantitative analysis were the ones measured using the portable sensor inside the climatic chamber (i.e., T_{amb} —air temperature inside the climatic chamber; RH_{amb} —relative humidity inside the climatic chamber). The temperatures measured with the two thermometers were differentiated by contact and non-contact (i.e., $T_{contact}$ —thermometer with contact; $T_{non-contact}$ —thermometer without contact).

2.4.2. Phase II: Evaluation of Thermal Comfort

During this phase, only the results from the IR camera 1 were used, since the face was more centrally framed in the images. The first analysis was targeted in the assessment of the heterogeneity of the temperature distribution throughout the face. To this end, six regions were defined, as represented in Figure 3 (1—face; 2—forehead; 3—cheekbone right; 4—cheekbone left; 5—nose; 6—chin).

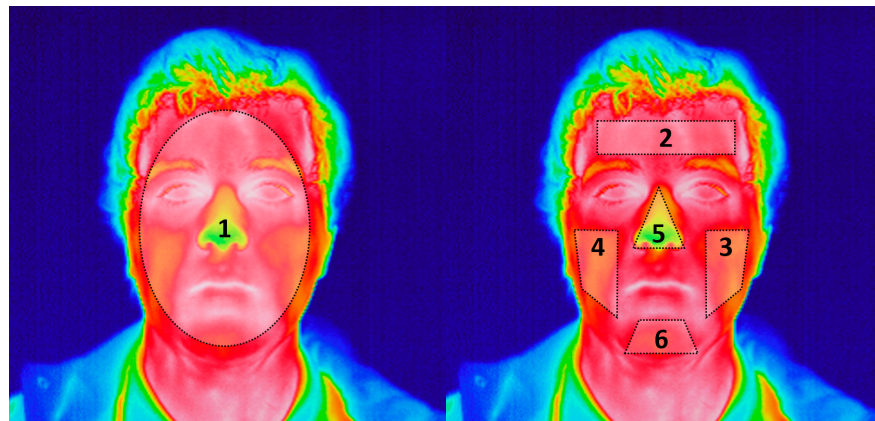


Figure 3. Regions of interest defined for the evaluation of thermal comfort: 1—face; 2—forehead; 3—cheekbone right; 4—cheekbone left; 5—nose; 6—chin.

In the second analysis, a possible correlation with the PMV model was tested. The PMV index was calculated according to ISO 7730 [27] and ASHRAE 55 [28]. The three clothing combinations resulted in the following insulation values: (i) 1.13 clo, when the T_{SP} values ranged between 10 °C and 14 °C; (ii) 0.83 clo, when the T_{SP} values ranged between 16 °C and 24 °C; (iii) 0.63 clo, when the T_{SP} values ranged between 26 °C and 30 °C. The metabolism was set as 1.0 met.

3. Results of Phase I: IR Camera Comparison

3.1. Qualitative Analysis

The qualitative analysis exposed different thermal patterns throughout the experiment, highlighting the impacts of the ambient conditions on the face temperatures, as presented in Figure 4. By analyzing the evolution of the face temperatures with the increase in T_{SP} , the thermal images show that for lower T_{SP} values, the temperatures are more heterogeneous, with the nose and cheekbones being the coldest regions and the mouth and the inner corner eye being the hottest regions. As the T_{SP} increases, the nose displays the largest temperature variation, followed by the cheekbones, which exhibit similar values on both sides. The forehead also displays high temperature values, especially at the extremities. Quite unexpectedly, the chin region also displays a high temperature, identical to the forehead, which is related to the use of a face mask (due to COVID-19 restrictions) during the intervals between the different tested scenarios, which is in line with the results found by Angelova and Velichkova [26]. For higher T_{SP} values, the face temperatures become more homogeneous, with little difference between distinct regions. This increased homogeneity occurs approximately when the T_{SP} reaches 26 °C. Similar results were reported by Sakoi et al. [12]. On the other hand, Figure 5 shows that there is no evident impact of RH_{SP} in the results, as for the same T_{SP} value, the thermal patterns are identical. The findings of the qualitative analysis are visible in the images captured with both IR cameras, even in the ones obtained with IR camera 2, which were not centrally framed.

3.2. Quantitative Analysis

3.2.1. Impacts of the Ambient Conditions on the Superficial Temperature

Figure 6 shows the box plot representations of the ambient and setpoint conditions and the reflected temperatures. The setpoint values (T_{SP} and RH_{SP}) slightly differ from the measured ambient values (T_{amb} and RH_{amb}), particularly for the lower setpoint values. These small differences can be explained by heterogeneities inside the climatic chamber.

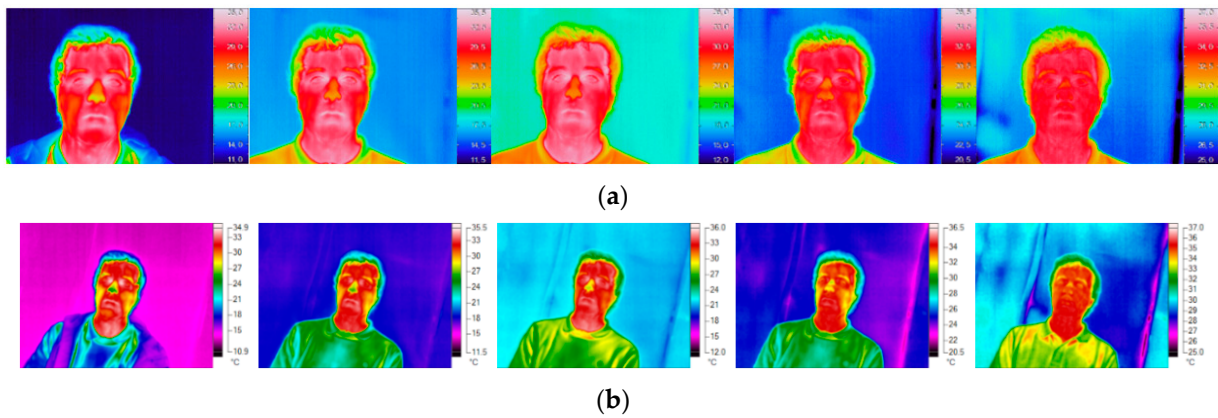


Figure 4. Thermal images for T_{SP} values of 10 °C, 16 °C, 20 °C, 24 °C, and 30 °C with an HR_{SP} of 60%: (a) IR camera 1; (b) IR camera 2.

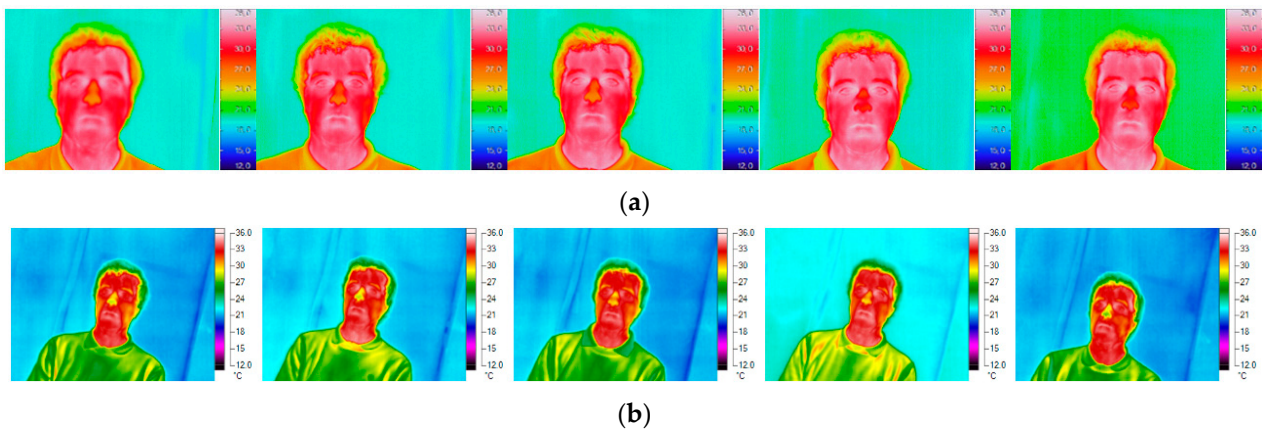


Figure 5. Thermal images for HR_{SP} values of 40%, 50%, 60%, 70%, and 80% with a T_{SP} of 20 °C: (a) IR camera 1; (b) IR camera 2.

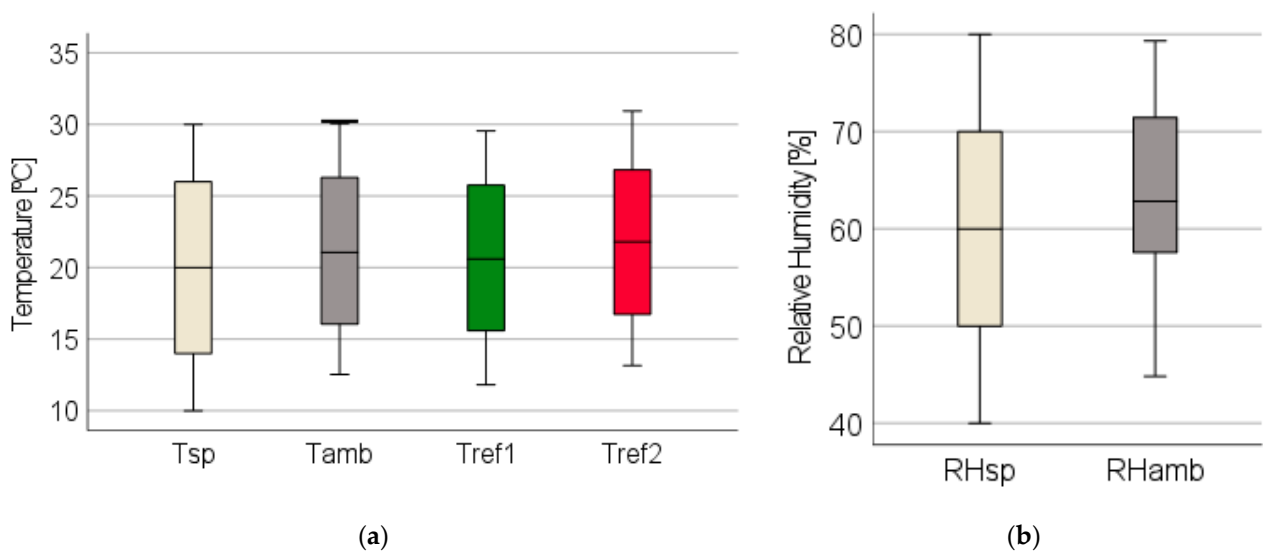


Figure 6. Box plots representations of (a) temperature and (b) relative humidity.

The reflected temperatures assessed by each IR camera (T_{ref1}—reflected temperature measured with IR camera 1; T_{ref2}—reflected temperature measured with IR camera 2) presents similar intervals ranges, with slightly higher values being measured by IR camera

2. Overall, the average values of the reflected temperatures are identical to the T_{amb} values; therefore, one can conclude that the impact of reflection was successfully minimized.

Figure 7 presents the distribution of the temperatures measured using the thermometers and the maximum temperature obtained using IRT. The results show that the core temperature (measured by the contact thermometer) is consistently higher than those measured by the other devices. The variability of the results attained with the contact thermometer is considerably lower, confirming the higher reliability of the measurements carried out with this device. Although operating based on the same physical principles, the non-contact thermometer presents higher variability than the IR cameras. The maximum temperature measured by IR camera 2 is always higher than the values obtained with IR camera 1. The t -test confirmed the statistically significant differences between the 2 IR cameras (t -test = 4.248; p -value < 0.01%). This result points to a possible impact of the camera position.

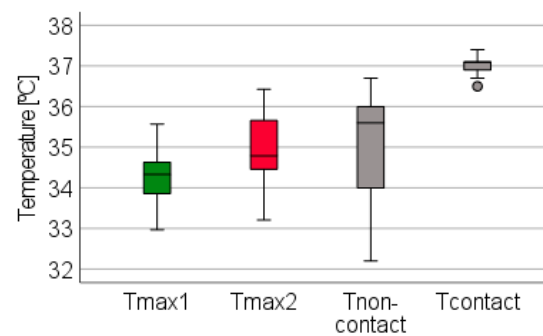


Figure 7. Box plots representation of the maximum temperatures measured with IR cameras and thermometers (HR_{SP} values of 40%, 60% and 80%).

3.2.2. Location of the Hottest Point

The next step was the detection of the locations of the hottest points measured by the IR cameras. Generally, four different positions were found, as presented in Figure 8a. In the mouth and the eyes, the position of the hottest point often changed between the right and left extremities. IR camera 2 identified the chin as the hottest point in two occurrences. No association was found between the location of the hottest point and the setpoint values, with the positions randomly varying within the face, regardless of the temperature or relative humidity.

The two IR cameras showed good agreement, identifying the same position in most of the tests. Figure 8b highlights this finding, as a total of 69 scenarios out of 99 present the same location. According to the findings of Metzmacher et al. [13], the inner eye corner is the region with the highest temperature. This was only partially observed in the results, since the largest number of occurrences was in the mouth, followed by the eyes and forehead. This difference could mean that the 10 min period of acclimatization is insufficient to mitigate the effects of the face mask.

In order to confirm the association between the positions of the hottest points identified by the IR cameras, a chi-squared test was performed. In this test, the null hypothesis was “ H_0 : there is no association” and the significance level applied was $\alpha = 5\%$. The result was 53.33 with a p -value < 0.01%, meaning there was an association between the results of the two IR cameras.

3.2.3. Statistical Analysis

Table 2 presents the values of the linear correlation coefficient, r (p -value), between the following variables: (i) the measured ambient conditions (T_{amb} and RH_{amb}); (ii) the temperatures of the hottest points (T_{max1} and T_{max2}); (iii) the reflected temperatures (T_{ref1} and T_{ref2}).

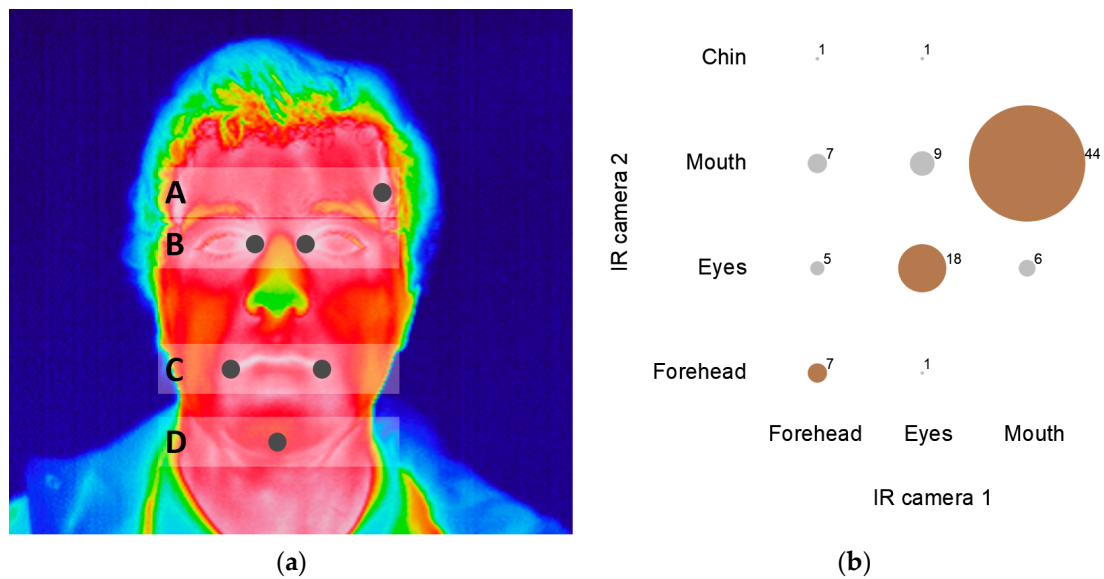


Figure 8. Locations of the hottest points in the face: (a) A—forehead; B—eyes; C—mouth; D—chin; (b) association between IR cameras.

Table 2. Pearson’s correlation matrix.

	T_{amb}	RH_{amb}	T_{max1}	T_{max2}	T_{ref1}	T_{ref2}
T_{amb}	1.000	0.093 (0.361)	0.886 (0.000)	0.918 (0.000)	0.999 (0.000)	0.996 (0.000)
RH_{amb}		1.000	0.144 (0.156)	−0.062 (0.544)	0.115 (0.256)	0.130 (0.200)
T_{max1}			1.000	0.842 (0.000)	0.890 (0.000)	0.882 (0.000)
T_{max2}				1.000	0.915 (0.000)	0.906 (0.000)
T_{ref1}					1.000	0.997 (0.000)
T_{ref2}						1.000

The results show that there is no significant correlation between the RH_{amb} and the other variables for a significance level of 5%, which indicates that the RH_{amb} does not influence the face temperature results, being in concordance with the qualitative analysis discussed in Section 3.1. The remaining variables are strongly correlated with each other. One should stress that the linear correlation coefficient is greater than 0.996 for the relationships between T_{amb} , T_{ref1} , and T_{ref2} , which is in concordance with Figure 6a and confirms the non-existence of reflection problems.

Figure 9a represents the variation of the box plot representations of the maximum temperatures (T_{max}) within the range of T_{SP} values. The two IR cameras follow the same trend, although IR camera 2 shows larger variability and slightly higher temperatures, with an average temperature approximately 0.5 °C above IR camera 1. Figure 9b shows that the impact of the relative humidity can be neglectable, as previously discussed. Throughout the range of relative humidity values, both the average value and the variability of the face maximum temperature are similar in the two devices.

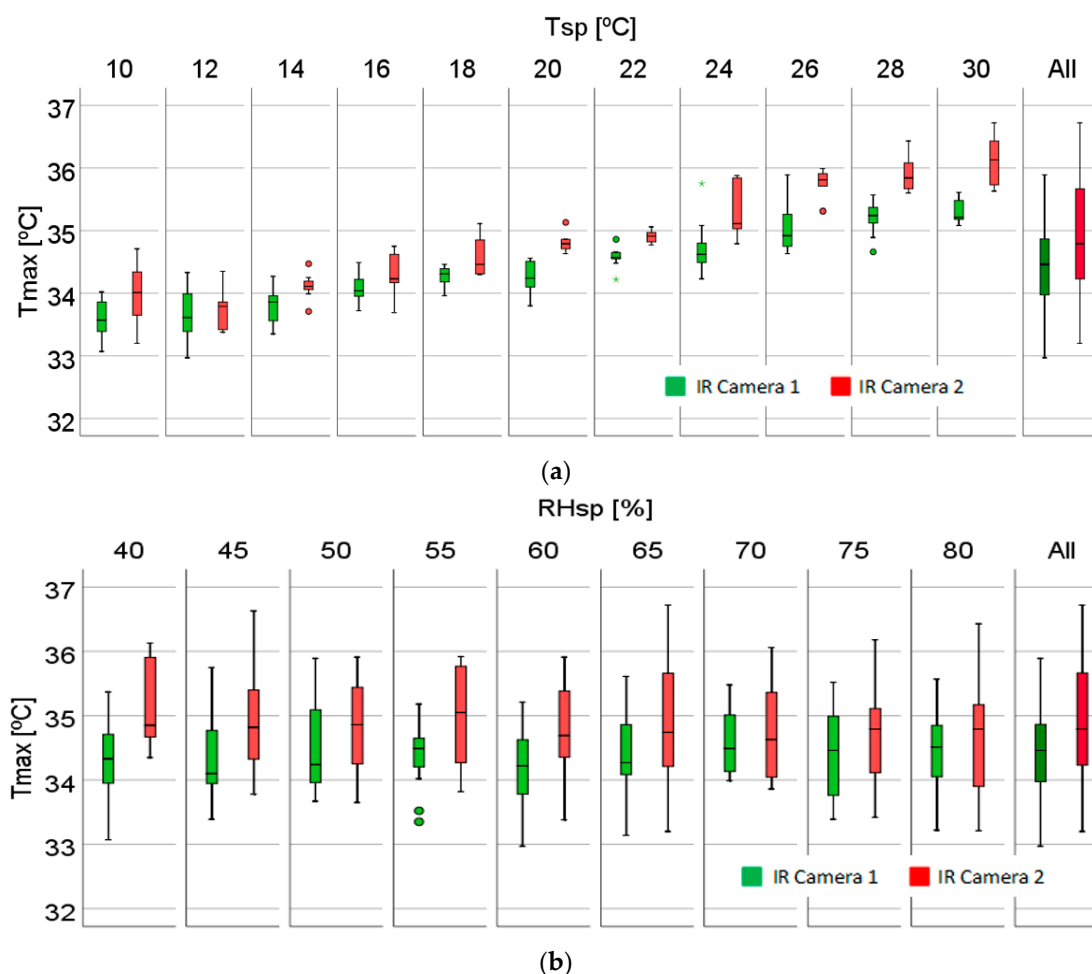


Figure 9. Box plot representations of the maximum temperatures for the entire range: (a) T_{SP} ; (b) RH_{SP} .

4. Results of Phase II: Evaluation of Thermal Comfort

4.1. Temperature Variation within the Face

The preliminary step to evaluate thermal comfort using IRT is to evaluate the heterogeneity of the temperature on the face. For this purpose, the methodology presented in Section 2.4.2 and Figure 3 was implemented. Figure 10 presents the box plots of the maximum (Figure 10a), minimum (Figure 10b), and average (Figure 10c) temperature distributions within the six regions of the face, throughout the range of TSP values. As expected, all of the different regions display an increase in temperature with the increase in T_{SP} . However, among them, some relevant differences can be noticed, reinforcing the findings discussed in Section 3.1.

Considering the maximum and minimum values, one can conclude that the former occur somewhere outside the five subregions considered here (box plots 2 to 6 in Figure 10a), while the latter are on the nose (box plots 1 and 6 in Figure 10b). In fact, the previous analysis already showed that the maximum temperature occurs in the inner eye corner or in the mouth (Figure 8).

Regarding the average temperatures (Figure 10c), with the lower T_{SP} values, the heterogeneity is more obvious, with the nose having the most extreme discrepancy in comparison with the other regions, always presenting lower temperatures (box plot 5). Both cheekbones exhibit similar temperatures (box plots 3 and 4), which are higher than the nose but lower than the other regions. Low temperatures in the nose were already reported in the literature [15,17]. However, according to the same authors, the values should be closer to the ones on the cheekbones. One possible explanation for this may be the limits

defined for the area that represents the cheekbones, which were small in this case study and might not have included the cooler zones. The forehead and chin (box plots 2 and 6) are the regions with the highest values, with the chin exhibiting slightly higher temperatures.

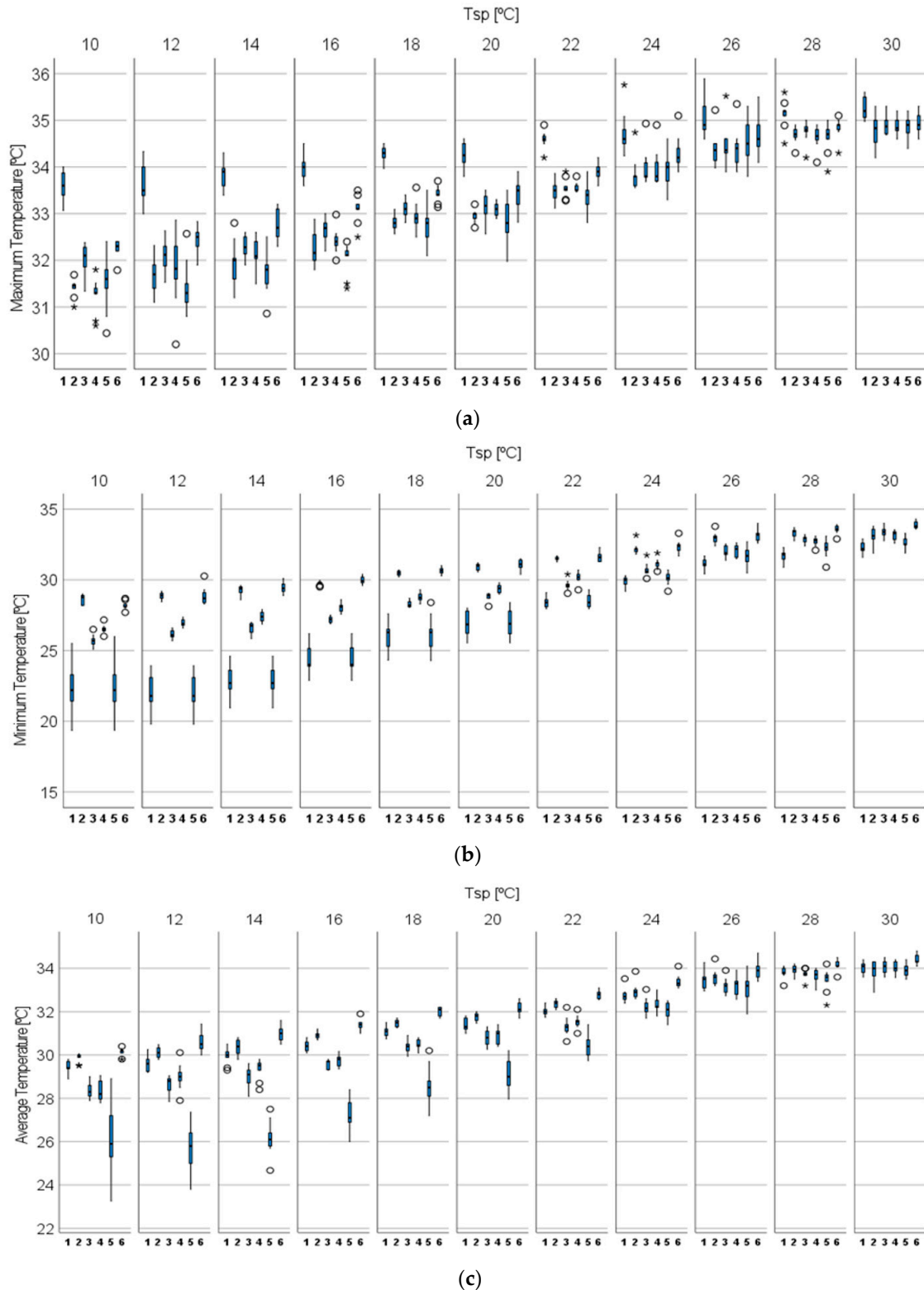


Figure 10. Box-plot representations: (a) maximum temperature; (b) minimum temperature; (c) average temperature for each region (1—face; 2—forehead; 3—cheekbone right; 4—cheekbone left; 5—nose; 6—chin).

At intermediate T_{SP} values, the dispersion of temperatures between regions becomes less marked. The nose remains the region with the lower temperature, in clear contrast with the homogeneity presented by the other regions. In fact, all regions exhibit closer temperature values and the relative differences between them remain unchanged. At higher temperature values, there is a clear increase in the homogeneity of the temperatures of the regions. This phenomenon starts occurring when the T_{SP} reaches 26 °C.

4.2. Face Temperature vs. PMV

For each tested scenario, the PMV value was calculated and its relationship with the average temperature for the six regions of the face was assessed. Figure 11 depicts the scatter plot of the results and Table 3 shows the linear regression analysis applied to each region. Both highlight the strong linear relation between the PMV and average temperature values in all subregions and for the face as a whole. This is confirmed by the goodness of fit of each linear model, R^2 , which presents values higher than 89%. However, due to the greater variability in this subregion, the robustness of the linear relation between the PMV and average temperature on the nose is lower than in other regions. The best result occurs in the cheekbones, with a higher R^2 value, even if the chin and forehead have the lowest variations in temperature (Figure 10c). A strong relation was also found when the entire face was considered ($R^2 = 93.3\%$), which is important, since the use of this region is easier to implement in practice. Therefore, the average facial temperature can be used as an indicator for the determination of thermal comfort, while an evaluation of the individual subregions is not necessary.

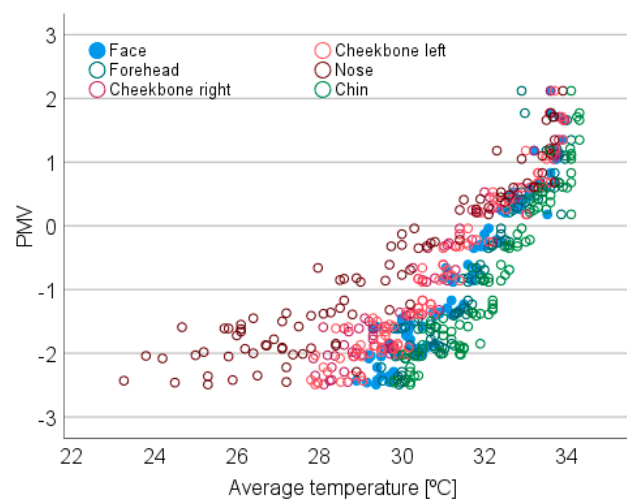


Figure 11. Relations between PMV values and average temperatures for the six regions of the face.

Table 3. R^2 and linear tendency lines for the six regions of the face.

	Face	Forehead	Cheekbone Left	Cheekbone Right	Nose	Chin
Constant	-25.74	-28.56	-20.98	-21.99	-12.73	-29.56
Slope	0.80	0.88	0.66	0.69	0.41	0.90
R^2	93.3%	90.4%	93.9%	93.7%	89.1%	91.8%

4.3. Prediction Model for PMV Based on IRT

The results obtained via IRT were used to propose a prediction model for PMV. Figure 12 shows the linear relation between the PMV and mean face temperature as measured using IRT, including the fitted model line and the 95% confidence interval for the predicted values. According to the model, the PMV index can be estimated using

Equation (1). The proposed model has a root mean square error close to 0.70. The range of application of the model is limited to the face temperature range of 28.9 °C to 34.4 °C.

$$PMV = -25.740 + 0.796 \times T_{face} \quad (1)$$

One should stress that the generalization of the model requires further research. Increasing the size of the sample will allow the accuracy of the model to be fine-tuned. Aspects such as the age, gender, and weight are commonly referred to in the literature [29,30] as impacting thermal comfort and should, therefore, be taken into account. Afterwards, the validation of the model must be carried out in real environmental conditions, including the definition of the limit conditions of its implementation and the establishment of the test protocol.

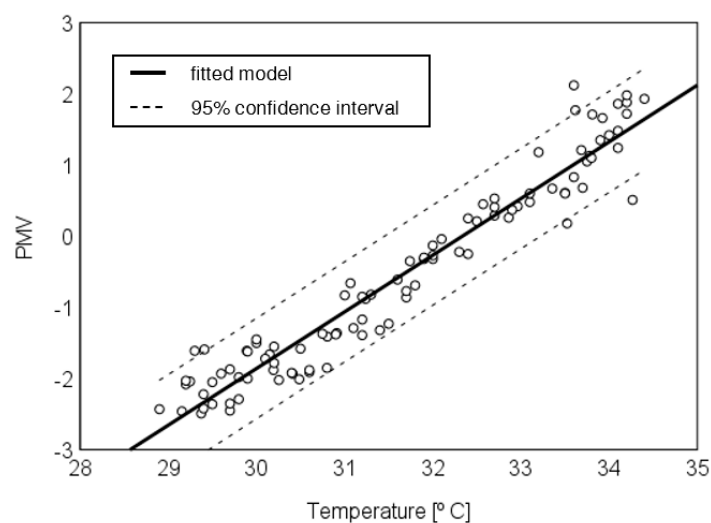


Figure 12. PMV prediction model as a function of the average face temperature.

5. Conclusions

This work has allowed a better understanding of several issues related to the measurement of face temperatures using IRT. It shows that face temperatures are more heterogeneous at lower air temperatures and the thermal patterns become more homogeneous above 26 °C. On the other hand, there are no evident impacts of the relative humidity on the temperature of the face, nor on its thermal patterns. The core temperature, as measured by the contact thermometer, was consistently higher than the one measured with the IR cameras, which was expected. However, the results also confirmed the reliability and consistency of the measurements carried out using IRT.

Regarding the results obtained with the two IR cameras, they were similar in terms of the qualitative analysis but were more clearly marked in the images where the face was more centrally framed. Furthermore, the position of the hottest point on the face pointed to a statistically significant association when assessed with the two IR cameras. From these results, the maximum temperatures on the face as measured by the two IR cameras were statistically different, pointing to an impact of the camera position.

The hottest points on the face were mostly located in the mouth, followed by the eyes and forehead. The lower temperatures always occurred on the nose, but the differences from the other subregions tended to attenuate when the air temperature increased. The average facial temperature can be used as an indicator for the determination of the face temperature, while an evaluation of the individual subregions is unnecessary, which indicates that it can be used as a parameter for the determination of thermal comfort.

A strong relation was found between the PMV and the temperature of the entire face ($R^2 = 93.3\%$), which allowed us to establish an innovative prediction model for PMV based on the IRT results. The model presented a root mean square error close to 0.70 when applied

in a face temperature range between 28.9 °C and 34.4 °C. The encouraging results that were produced by this work will enable us to proceed to the next stage, which will involve the generalization of the model by increasing the size of the sample and including aspects such as the type of skin, age, gender, and weight, which will allow us to fine-tune its accuracy. By expanding the sample size, special attention can be paid to the impacts of gender and age, which are typically pointed out as factors that influence the perception of comfort. The airflow and the view angle of the IRT camera are also possible sources of uncertainty that must be taken into consideration in the following steps of the research. Afterwards, the validation of the model must be carried out in real environmental conditions.

Author Contributions: Conceptualization, R.M.S.F.A. and E.B.; methodology, R.M.S.F.A. and E.B.; formal analysis, R.M.S.F.A., E.B., M.L.S. and T.S.F.S.; resources, R.M.S.F.A. and E.B.; data curation, M.L.S. and T.S.F.S.; writing—original draft preparation, T.S.F.S.; writing—review and editing, R.M.S.F.A., E.B. and M.L.S. All authors have read and agreed to the published version of the manuscript.

Funding: This work was financially supported by Base Funding UIDB/04708/2020 of the CONSTRUCT Instituto de I and D em Estruturas e Construções, funded by national funds through FCT/MCTES (PIDDAC), and by the “Protocolo de medição da temperatura corporal através da termografia de infravermelhos—IRT4COVID19” research project under the scope of “Apoios Especiais do Instituto Politécnico de Viseu, despacho n° 59/2020 de 15-09-2020”.

Institutional Review Board Statement: Not applicable.

Informed Consent Statement: Informed consent was obtained from all subjects involved in the study.

Data Availability Statement: Not applicable.

Conflicts of Interest: The authors declare no conflict of interest.

References

1. Balaras, C.A.; Argiriou, A.A. Infrared thermography for building diagnostics. *Energy Build.* **2002**, *34*, 171–183. [[CrossRef](#)]
2. Cheung, M.Y.; Chan, L.S.; Lauder, I.J.; Kumana, C.R. Detection of body temperature with infrared thermography: Accuracy in detection of fever. *Hong Kong Med. J.* **2012**, *18*, 31–34. [[PubMed](#)]
3. Lahiri, B.B.; Bagavathiappan, S.; Jayakumar, T.; Philip, J. Medical applications of infrared thermography: A review. *Infrared Phys. Technol.* **2012**, *55*, 221–235. [[CrossRef](#)] [[PubMed](#)]
4. Tanda, G. Skin temperature measurements by infrared thermography during running exercise. *Exp. Therm. Fluid Sci.* **2016**, *71*, 103–113. [[CrossRef](#)]
5. Takada, S.; Matshumoto, S.; Matshushita, T. Prediction of whole-body thermal sensation in the non-steady state based on skin temperature. *Build. Environ.* **2013**, *68*, 123–133. [[CrossRef](#)]
6. Liu, W.; Lian, Z.; Deng, Q.; Liu, Y. Evaluation of calculation methods of mean skin temperature for use in thermal comfort study. *Build. Environ.* **2011**, *46*, 478–488. [[CrossRef](#)]
7. Liu, W.; Tian, Z.; Yang, D.; Deng, Y. Evaluation of individual thermal sensation at raised indoor temperatures based on skin temperature. *Build. Environ.* **2021**, *188*, 107486. [[CrossRef](#)]
8. Choi, J.-H.; Loftness, V. Investigation of human body skin temperatures as a bio-signal to indicate overall thermal sensations. *Build. Environ.* **2012**, *58*, 258–269. [[CrossRef](#)]
9. Chaudhuri, T.; Zhai, D.; Soh, Y.C.; Li, H.; Xie, L. Thermal comfort prediction using normalized skin temperature in a uniform built environment. *Energy Build.* **2018**, *159*, 426–440. [[CrossRef](#)]
10. Chaudhuri, T.; Soh, Y.C.; Li, H.; Xie, L. Machine learning driven personal comfort prediction by wearable sensing of pulse rate and skin temperature. *Build. Environ.* **2020**, *170*, 106615. [[CrossRef](#)]
11. Sakoi, T.; Tsuzuki, K.; Kato, S.; Ookam, R.; Song, D.; Zhu, S. Thermal comfort, skin temperature distribution, and sensible heat loss distribution in the sitting posture in various asymmetric radiant fields. *Build. Environ.* **2007**, *42*, 3984–3999. [[CrossRef](#)]
12. Aryal, A.; Becerik-Gerber, B. A comparative study of predicting individual thermal sensation and satisfaction using wrist-worn temperature sensor, thermal camera and ambient temperature sensor. *Build. Environ.* **2019**, *160*, 106223. [[CrossRef](#)]
13. Metzmacher, H.; Wölki, D.; Schmidt, C.; Frisch, J. Real-time human skin temperature analysis using thermal image recognition for thermal comfort assessment. *Energy Build.* **2018**, *158*, 1063–1078. [[CrossRef](#)]
14. Ghahramani, A.; Castro, G.; Becerik-Gerber, B.; Yu, X. Infrared thermography of human face for monitoring thermoregulation performance and estimating personal thermal comfort. *Build. Environ.* **2016**, *109*, 1–11. [[CrossRef](#)]
15. Li, D.; Menassa, C.C.; Kamat, V.R. Non-intrusive interpretation of human thermal comfort through analysis of facial infrared thermography. *Energy Build.* **2018**, *176*, 246–261. [[CrossRef](#)]

16. Ghahramani, A.; Castro, G.; Karvigh, S.A.; Becerik-Gerber, B. Towards unsupervised learning of thermal comfort using infrared thermography. *Appl. Energy* **2018**, *211*, 41–49. [[CrossRef](#)]
17. Tejedor, B.; Casals, M.; Gangoellés, M.; Macarulla, M.; Forcada, N. Human comfort modelling for elderly people by infrared thermography: Evaluating the thermoregulation system responses in an indoor environment during winter. *Build. Environ.* **2020**, *186*, 107354. [[CrossRef](#)]
18. Cosma, A.C.; Simha, R. Thermal comfort modeling in transient conditions using real-time local body temperature extraction with a thermographic camera. *Build. Environ.* **2018**, *143*, 36–47. [[CrossRef](#)]
19. Loredan, N.P.; Lipovac, D.; Jordan, S.; Burnard, M.D.; Sarabon, N. Thermal effusivity of different tabletop materials in relation to users' perception. *Appl. Ergon.* **2022**, *100*, 103664. [[CrossRef](#)]
20. Li, D.; Menassa, C.C.; Kamat, V.R. Personalized human comfort in indoor building environments under diverse conditioning modes. *Build. Environ.* **2017**, *126*, 304–317. [[CrossRef](#)]
21. Li, X.; Chen, Q. Development of a novel method to detect clothing level and facial skin temperature for controlling HVAC systems. *Energy Build.* **2021**, *239*, 110859. [[CrossRef](#)]
22. Li, P.; Dai, P.; Cao, D.; Liu, B.; Lu, Y. Non-intrusive comfort sensing: Detecting age and gender from infrared images for personal thermal comfort. *Build. Environ.* **2022**, *219*, 109256. [[CrossRef](#)]
23. Yi, C.; Childs, C.; Peng, C.; Robinson, D. Thermal comfort modelling of older people living in care homes: An evaluation of heat balance, adaptive comfort, and thermographic methods. *Build. Environ.* **2022**, *207*, 108550. [[CrossRef](#)]
24. Fernández-Cuevas, I.; Bouzas Marins, J.C.; Arnáiz Lastras, J.; Gómez Carmona, M.; Piñonosa Cano, S.; Ángel García-Concepción, M.; Sillero-Quintana, M. Classification of factors influencing the use of infrared thermography in humans: A review. *Infrared Phys. Technol.* **2015**, *71*, 28–55. [[CrossRef](#)]
25. ASTM: E 1862-97; Standard Test Methods for Measuring and Compensating for Reflected Temperature Using Infrared Imaging Radiometers. American Society for Testing and Materials: West Conshohocken, PA, USA, 2010.
26. Angelova, R.A.; Velichkova, R. Using face masks in the classroom: The effect on the indoor environment parameters and face thermophysiological reactions. *Appl. Ecol. Environ.* **2022**, *20*, 135–151. [[CrossRef](#)]
27. ISO 7730: 2005; Ergonomics of the Thermal Environment-Analytical Determination and Interpretation of Thermal Comfort Using Calculation of the PMV and PPD Indices and Local Thermal Comfort Criteria. International Organization for Standardization: Geneva, Switzerland, 2005.
28. *Thermal Environmental Conditions for Human Occupancy*; ASHRAE: Peachtree Corners, GA, USA, 2013; Volume 55.
29. Almeida, R.M.S.F.; Ramos, N.M.M.; Freitas, V. Thermal comfort models and pupils' perception in free-running school buildings of a mild climate country. *Energy Build.* **2016**, *111*, 64–75. [[CrossRef](#)]
30. Cardoso, V.; Ramos, N.M.M.; Almeida, R.M.S.F.; Barreira, E.; Martins, J.P.; Simões, M.L.; Sanhudo, L. A discussion about thermal comfort evaluation in a bus terminal. *Energy Build.* **2018**, *168*, 86–96. [[CrossRef](#)]